

ROBUST OPTICAL 2D PERMEABILITY CHARACTERIZATION OF REINFORCING FABRICS

E. Fauster¹, H. Grössing², K. Fellner³ and R. Schledjewski^{1,2}

¹Chair of Processing of Composites, Department Polymer Engineering and Science,
Montanuniversität Leoben, Otto Glöckel-Str. 2/III, 8700 Leoben, Austria

²Christian Doppler Laboratory for High Efficient Composite Processing,
Montanuniversität Leoben, Otto Glöckel-Str. 2/I, 8700 Leoben, Austria

³Polymer Competence Center Leoben, Roseggerstraße 12, 8700 Leoben, Austria

Keywords: Liquid Composite Molding, Optical Permeability Characterization, Digital Image Processing

Abstract

Two-dimensional optical permeability characterization involves a glass plate as optically transparent mold half in order to enable visual observation of the advancing flow front. Due to comparatively low structural stiffness of the glass plate, deformation occurs as a result of mechanical loading, which is a combination of preform compaction pressure and fluid pressure. The glass plate deformation causes unwanted effects for the experiment and distorts the resulting in-plane permeability values.

The paper at hand presents a new approach for compensating these effects involving a combination of image and data processing steps with structural FEM simulation in a fully automated evaluation procedure. The basic concept of this approach is presented together with details on the particular working steps.

1. Introduction

In liquid composite molding (LCM), dry preforms of reinforcing fabrics are placed in a mold and then impregnated with the liquid polymer matrix material. The impregnation process plays a key role as insufficiently saturated regions directly affect the mechanical properties of the final component. In order to avoid elaborate and expensive impregnation trials, filling simulations can be accomplished. These simulations strongly rely on accurate and trustworthy permeability values. A well-known approach to determine 2-dimensional permeability values of reinforcing fabrics is based on the observation of radial flow experiments (see Figure 1). There, a three-stage data evaluation procedure is followed: (1) acquisition of specific sensor data during the actual experiment, (2) evaluation of the sensor data to determine the timely flow front advancement and (3) calculation of the 2D permeability values from these characteristics [1–3].

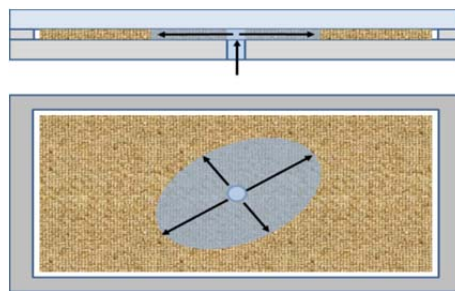


Figure 1. Schematics of a radial flow experiment.

In this work, which represents a continuation of an analysis previously presented by the authors [4], two different approaches for capturing the 2-dimensional flow front during the radial flow experiments are addressed: an optical and a capacitive measurement technique. The optical approach relies on a camera system focusing on the reinforcing fabric, which is positioned in a cavity with an optically transparent mold half, i.e. a glass plate. The capacitive measurement technique involves a set of linear dielectric sensors, which are oriented in a star-like scheme around the central injection opening. The sensors capture a dielectric entity which increases linearly as the fluid saturates the sensitive sensor area. For both techniques, the flow front is finally reconstructed by data interpolation or approximation strategies, respectively.

As the optical technique requires a glass plate, the structural stiffness of the mold is significantly lower than in the capacitive setup, where a full-metal mold is used. As a result, the load acting on the glass plate, which is a combination of the preform compaction pressure and the pressure field of the injected test fluid, can easily lead to a deformation of the cavity. This obviously affects the measurement results. In this paper, a strategy for compensating the distorted permeability results based on the loading situation and the cavity deformation characteristics is presented. The method involves a mechanical FEM simulation model describing the cavity deformation as a result of preform compaction and fluid pressure.

2. Testrig Description

Figure 2 shows a picture of the optical test rig used for this work. The frame of the test rig is set up by standard aluminum profiles. Directly on top of the working table, the metal mold half is mounted. The security glass plate forming the upper mold half is made from two glass plates, each 19 mm in thickness, separated by a 0.76 mm thin polymer foil. The glass mold half is framed with metal profiles in order to connect it to a hinge system on the back side of the test rig. A pneumatic cylinder finally provides for the flapping motion of the glass plate.

The actual mold cavity is specified through the cavity frame showing an inner dimension of 300 mm x 400 mm. After placing the reinforcing structures inside the cavity, the mold is closed by flapping the glass plate into a horizontal position. In addition, the glass plate is tightened with the lower mold half using a metal clamping frame and a set of screws. The radial flow experiment is then executed by injecting the test fluid into the cavity through a central injection point in the metal bottom mold half.

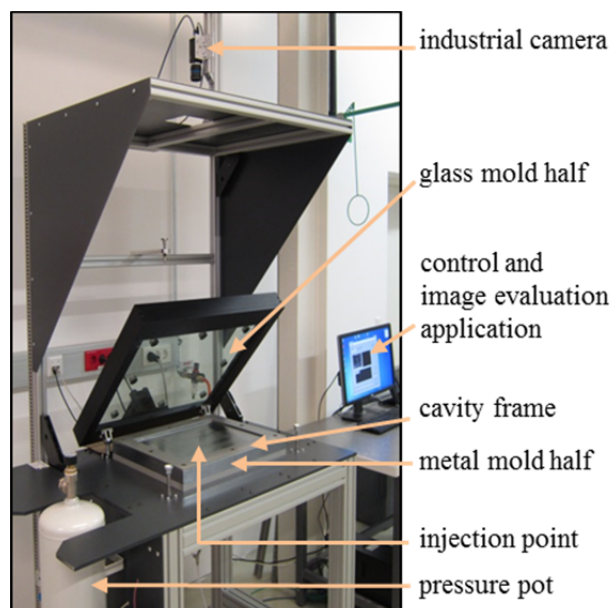


Figure 2. Optical permeability measurement system used for the radial flow experiments.

At a distance of about 1 m above the mold, a camera system consisting of an industrial monochrome camera and a precision lens with a focal length of 16 mm is mounted. The camera is used to acquire an image sequence during the radial flow experiment at an acquisition rate of up to 50 fps at a resolution of 1392 x 1040 pixels.

3. Data Evaluation Strategy

The schematic depicted in Figure 3 gives an overview of the particular steps followed in the data evaluation procedure in order to determine in-plane permeability values involving the deformation of the glass plate as a result of the mechanical loading through preform compaction pressure and fluid injection pressure. This procedure is executed individually for all of the sequence images acquired during the radial flow experiment.

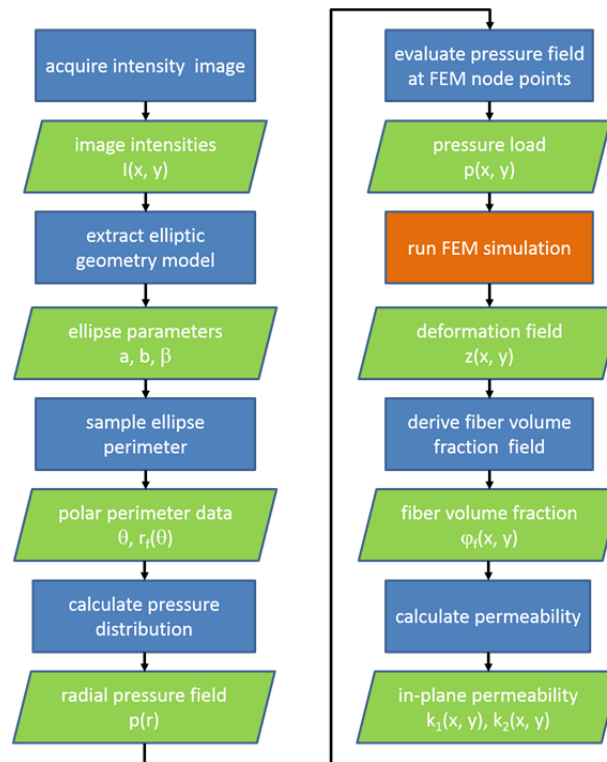


Figure 3. Flow diagram of the data evaluation procedure.

The FEM simulation was set up and run in the well know simulation platform Abaqus[®] from Dassault Systemes[®] (www.3ds.com), whereas all of the image and data processing steps were realized with Matlab[®], a technical computation software developed by MathWorks[®] (www.mathworks.com).

3.1. Image Processing and Elliptical Geometry Model Fitting

Each of the sequence images is evaluated by means of a digital image processing algorithm specifically developed for this application [5], resulting in an elliptical geometry model as shown in Figure 4. As can be seen, the ellipse is centered at the point of fluid injection. Choosing this as the point of origin, the model ellipse can be fully described with a set of three parameters: the semi-major and semi-minor axis lengths a and b , respectively, as well as the orientation angle β specified as the angle of the major ellipse axis with the horizontal image edge.

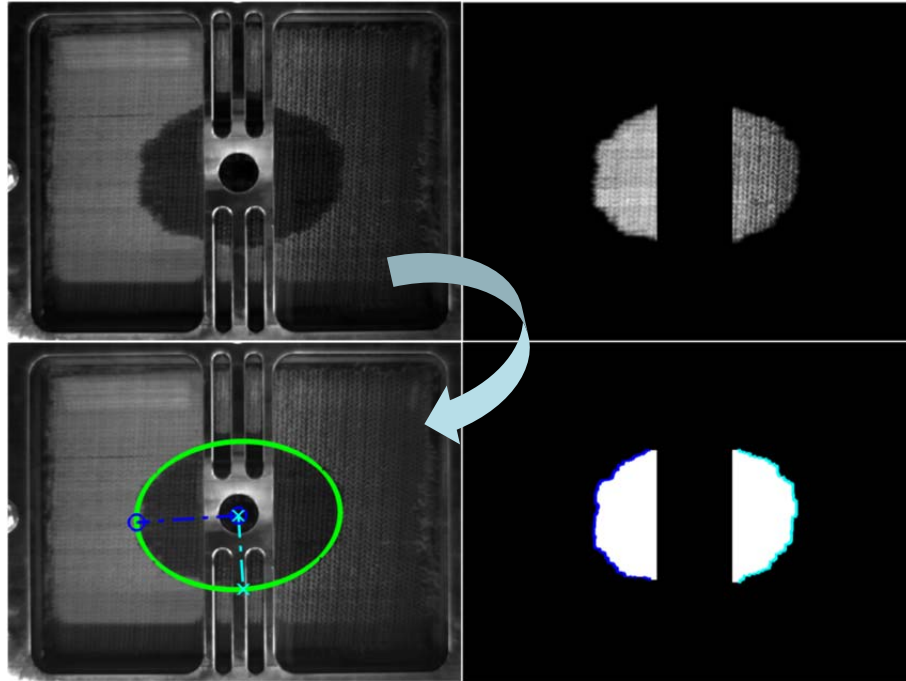


Figure 4. Example image of a radial flow experiment (top left) acquired with the optical permeameter and evaluation steps of the digital image processing algorithm (clockwise order).

As outlined by the authors in a previous work [4], the task of fitting an elliptical geometry model to a set of n noisy data points $p_i = [x_i, y_i]^T, i = [1..n]$, along the fluid flow front is described as a nonlinear least squares problem, which is solved by minimizing $\sum_{i=1}^n r_i^2$, i.e. the sum of squared data residuals r_i , which in turn represent algebraic distances of the data points p_i to the elliptic geometry model being sought. For our specific fitting problem with the ellipse centered at the point of origin, we end up with calculating the singular value decomposition [6] of a scatter matrix $S = D^T D$, which is calculated from a design matrix D holding the coordinates of the data points according to the following scheme:

$$D = \begin{bmatrix} x_1^2 & x_1 y_1 & y_1^2 \\ \vdots & \vdots & \vdots \\ x_n^2 & x_n y_n & y_n^2 \end{bmatrix}. \quad (1)$$

3.2. Polar Ellipse Perimeter Sampling

As this is required for the subsequent step of calculating the fluid pressure characteristics, the perimeter of the elliptical geometry model describing the fluid flow front is parameterized by means of polar coordinates $\{r_f, \theta\}$. The sampling angles $\theta_i = \frac{i\pi}{180}, i = \{1, 2, \dots, 360\}$ were chosen in a mathematically positive sequence with the 0° -direction aligned with the major ellipse axis. Then, the polar radii, i.e. the radial extent of the fluid flow front at certain sampling angles θ_i , are:

$$r_f(\theta_i) = \frac{b}{\sqrt{1 - \varepsilon^2 \cos^2 \theta_i}}, \quad (2)$$

with the squared eccentricity $\varepsilon^2 = \frac{a^2 - b^2}{a^2}$ as well as the semi-major and semi-minor axis lengths a and b , respectively [7].

3.3. Fluid Pressure

Along each of the polar rays connecting the point of origin with a sample point on the ellipse perimeter, the fluid pressure characteristics is modelled according to Weitzenböck [8] as follows:

$$p(r) = \begin{cases} p_0 & \dots r < r_0, \\ p_0 - (p_0 - p_f) \frac{\ln r - \ln r_0}{\ln r_f - \ln r_0} & \dots r_0 \leq r \leq r_f, \\ p_f & \dots r > r_f, \end{cases} \quad (3)$$

with the radius r_0 of the circular injection opening, the radial extent r_f of the flow front as well as the fluid injection pressure p_0 and the pressure p_f at the flow front. Note that for the analyses presented in this paper, p_f corresponds to ambient pressure. Collecting the pressure characteristics from all of the polar rays, a three-dimensional pressure field is obtained. Pressure characteristics of an exemplarily chosen flow front situation are visualized in Figure 5, whereas the pressure values are shown at dimensionless scale, i.e. $\hat{p} = \frac{p(r)-p_f}{p_0}$. The logarithmic nature of the pressure characteristics according to Equation (3) is obvious, i.e. the fluid pressure is concentrated to the close proximity of the injection opening.

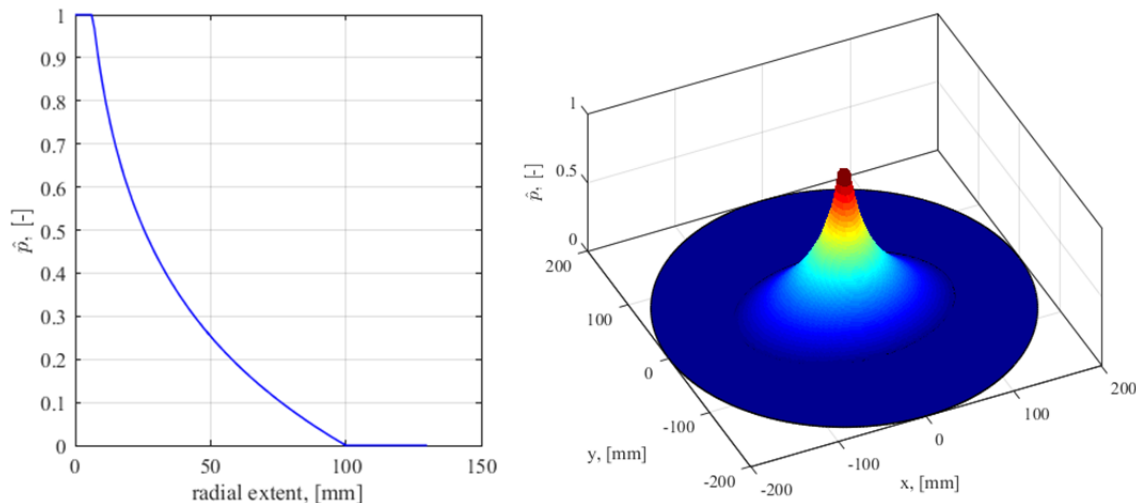


Figure 5. 2D pressure characteristics along a polar ray (left) and 3D distribution of the fluid pressure in anisotropic porous media (right).

3.4. Preform Compaction Pressure

When closing the mold of the optical permeameter, the preform located in the cavity is transversely compacted to obtain a certain level of fibre volume fraction in the preform. As discussed by Chen and Chou [9,10], the packing of the reinforcing fibres is affected by mechanisms at (a) micro-scale (rearrangement of fibres within a tow), (b) meso-scale (nesting of tows within single material layers) and (c) macro-scale (nesting of fibre tows from superimposed material layers). The compaction behaviour of reinforcing fabrics can easily be studied by means of compressibility tests, such as those presented by Lekakou et al. [11] or Chen et al. [12], resulting in compaction pressure characteristics depending on the fibre volume fraction as well as the number of material layers in the preform.

For the study described in this paper, preform compaction pressure was assumed to be uniform over the preform area. The actual compaction pressure values were derived from compressibility tests executed on a stack of reinforcing material with the number of preform layers equalling that of the preforms used for the permeability experiments.

The assumption of uniform preform compaction pressure does not fully reflect reality, as the cavity height is actually varying with in-plane location as a result of glass plate deformation, which in turn causes a variation of the local fibre volume fraction. Moreover, hydrodynamic effects along the saturated preform regions cause a decrease of compaction pressure as discussed by Becker et al. [13]. In order to concentrate on establishing the systematics of the data evaluation process described in this paper, the simplified model of preform compaction was chosen. However, the concept can be flexibly extended to involve a more accurate preform compaction pressure model.

3.5. FEM Simulation of Glass Plate Deformation

The FEM model set up in Abaqus[®] and used to compute the glass plate deformation as a result of mechanical loads from preform compaction pressure and fluid injection pressure, was presented in previous work of the authors [4, 14] together with a verification of its validity based on optical deformation measurement of the glass plate under load. Thus, details of the FEM model are omitted here due to space limitations.

In order to provide the mechanical load data required for running the structural FEM simulation, the fluid pressure characteristics were evaluated at all of the node points of the FEM model. This data was exported from Matlab[®] in terms of an Abaqus[®] input file together with the preform compaction pressure values. Then, the FEM simulation run was directly initiated from within Matlab[®] by means of a specifically prepared batch file. The results of the structural FEM analyses were finally exported in terms of an Abaqus[®] output file, which in turn was directly read back into Matlab[®]. This strategy enables to run the data and image processing steps together with the FEM simulation in a fully automated way through all of the sequence images acquired during the radial flow experiment.

The resulting deformation data of the glass plate is exemplarily shown in Figure 6. The deformation shows a dome-shaped surface as a result of the rigid fixation of the glass plate borders along the outer margin as provided by the metal stiffening frame screwed to the metal lower mold half.

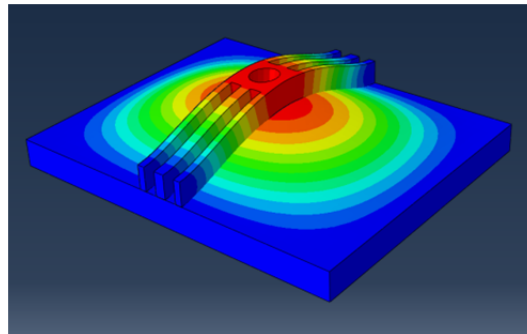


Figure 6. 3D visualization of the deformation of glass plate and metal stiffening frame as a result of to the combined load of preform compaction pressure and fluid injection pressure.

3.6. Fibre Volume Fraction

Considering the deformation surface of the glass plate as shown in Figur 6, the height h of the cavity obviously varies with the in-plane location, i.e. $h = h(x, y)$. Assuming the preform to properly follow this deformation as a result of stress relaxation effects, the fibre volume fraction of the reinforcing material in the cavity is locally varying as well, i.e.:

$$\varphi_f = \varphi_f(x, y) = \frac{n m_A}{h(x, y) \rho_f}, \quad (4)$$

with the number of preform layers n , the areal weight m_A of the fabric and the density ρ_f of the reinforcing fibers. Relating the extent of the flow front to the distribution of fibre volume fraction, we

can determine the local fibre volume fraction along the fluid flow front at every instant of the radial flow experiment.

3.7. In-Plane Permeability

Finally, the in-plane permeability values k_1 and k_2 were calculated according to the algorithm of Adams and Rebenfeld [15]. The algorithm is based on an iterative numerical solution for the degree of anisotropy $\alpha = \frac{k_2}{k_1}$ and requires knowledge about the following experimental parameters:

- i. cavity height h ,
- ii. number of material layers n ,
- iii. injection hole radius r_0 and
- iv. fluid injection pressure p_i

together with these material properties:

- v. fluid viscosity η ,
- vi. fabric areal weight m_A and
- vii. material density of the reinforcing fibers ρ_f .

Collecting the in-plane permeability values for all of the sequence images acquired during the radial flow experiment, k_1 and k_2 are obtained as timely varying properties. Associating these with the corresponding fibre volume fraction values finally results in a distribution of the in-plane permeability values, i.e. $k_1 = k_1(\varphi_f)$ and $k_2 = k_2(\varphi_f)$.

4. Summary and Future Work

This paper covers the concept of robust optical in-plane permeability determination by combination of experimental characterization work with analytic image and data processing as well as structural FEM simulation in a fully automated data processing procedure. Involving the FEM simulation allows for taking into account the deformation of the glass plate required for the optical setup when calculating in-plane permeability values. The paper outlines the basic concept of this approach and focusses on evaluation aspects of the particular image and data processing steps. Furthermore, the mathematical models used to describe preform compaction pressure as well as fluid pressure as contributors to the mechanical loads applied to the glass plate in the FEM simulation runs. Finally, the FEM model is briefly discussed together with the final data processing steps required to determine the in-plane permeability. Due to space limitations for this paper on the one hand as well as a lack of resilient results at the time of submitting this manuscript on the other hand (first results appearing very promising though), details on the evaluation results are omitted here but will be shown at the conference.

Future work is concentrating on involving more accurate models for preform compaction pressure as well as comparative analyses. These will compare the in-plane permeability results obtained with the data processing concept presented here with those of a global data evaluation procedure typically applied for this kind of experiment. Furthermore, a comparison of data obtained from optical and capacitive permeameter systems will be realized. This will reveal the potential of the data processing procedure to compensate for distorting effects of mold deformation in optical systems as the capacitive permeameter shows an ideally stiff, full-metal mold.

Acknowledgments

Ralf Schledjewski and Harald Grössing kindly acknowledge the financial support provided by the Federal Ministry of Science, Research and Economy in Austria and the FACC Operations GmbH.

Klaus Fellner is an employee of the Polymer Competence Center Leoben GmbH (PCCL, Austria). The PCCL is funded by the Austrian Government and the State Governments of Styria, Lower Austria and Upper Austria.

References

- [1] Adams KL, Rebenfeld L. Permeability characteristics of multilayer fiber reinforcements. Part I: Experimental observations. *Polymer Composites* 1991; 12(3):179–185.
- [2] Adams KL, Rebenfeld L. Permeability characteristics of multilayer fiber reinforcements. Part II: Theoretical model. *Polymer Composites* 1991; 12(3):186–190.
- [3] Bear J. *Dynamics of fluids in porous media*. New York: Dover; 1988.
- [4] Fauster E, Grössing H, Schledjewski R. A Comparison of Two Measurement Techniques for Determining the 2D Permeability Characteristics of Reinforcing Textiles. In: International Society of Composite Materials, editor. *Proceedings of 20th International Conference on Composite Materials*, Copenhagen, Denmark, 2015.
- [5] Fauster E, Grössing H, Schledjewski R. Uncertainty Analysis for Optical Permeability Measurement of Reinforcing Textiles. In: International Society of Composite Materials, editor. *Proceedings of 19th International Conference on Composite Materials*, Montreal, Canada, 2013.
- [6] Golub GH, van Loan CF. *Matrix computations*. 3rd ed. Baltimore: Johns Hopkins University Press; 1996.
- [7] Gallier JH. *Geometric methods and applications: For computer science and engineering*. New York: Springer; 2001.
- [8] Weitzenböck J, Sheno R, Wilson P. Measurement of three-dimensional permeability. *Composites Part A: Applied Science and Manufacturing* 1998(29A):159–169.
- [9] Chen B, Chou T. Compaction of woven-fabric preforms in liquid composite molding processes: single-layer deformation. *Composites Science and Technology* 1999; 59(10):1519–1526.
- [10] Chen B, Chou T. Compaction of woven-fabric preforms: nesting and multi-layer deformation. *Composites Science and Technology* 2000; 60(12-13):2223–2231.
- [11] Lekakou C, Johari, M. A. K., Bader MG. Compressibility and flow permeability of two-dimensional woven reinforcements in the processing of composites. *Polymer Composites* 1996; 17(5):666–672.
- [12] Chen B, Lang EJ, Chou T. Experimental and theoretical studies of fabric compaction behavior in resin transfer molding. *Materials Science and Engineering: A* 2001; 317(1-2):188–196.
- [13] Becker D, Mitschang P. Influence of Process Parameters on the Efficiency of Transverse Impregnation of Textiles. In: International Society of Composite Materials, editor. *Proceedings of 20th International Conference on Composite Materials*, Copenhagen, Denmark, 2015.
- [14] Grössing H. *Contributing to the Optimization of the Preform LCM Process Chain: Permeability of Reinforcing Textiles*. Dissertation. Leoben; 2015.
- [15] Adams KL, Russel W, Rebenfeld L. Radial penetration of a viscous liquid into a planar anisotropic porous medium. *International Journal of Multiphase Flow* 1988; 14(2):203–215.